Explicit wall models for large eddy simulation

Shang-Gui Cai, Pierre Sagaut

Explicit wall models for large eddy simulation

Shang-Gui Cai (蔡尚炅),[a] and Pierre Sagaut

AFFILIATIONS

Aix Marseille Univ, CNRS, Centrale Marseille, M2P2 UMR 7340, Marseille 13451, France

[a]Author to whom correspondence should be addressed: shanggui.cai@univ-amu.fr

ABSTRACT

Algebraic explicit wall models covering the entire inner region of the turbulent boundary layer are proposed to reduce the computational effort for large eddy simulation of wall-bounded turbulent flows. The proposed formulas are given in closed forms with either logarithmic- or power-function-based laws of the wall, allowing straightforward evaluation of the friction velocity on near wall grids independent of their locations in the turbulent boundary layer. The performance of the proposed models is demonstrated by the wall modeled large eddy simulation of a turbulent plane channel flow.

The large eddy simulation (LES) has been recognized as a powerful technique for predicting turbulent flows.[1,2] It captures the unsteady features more accurately than the (unsteady) Reynolds-averaged Navier–Stokes (RANS) equations while it is less expensive compared to the direct numerical simulation (DNS). However, in the case of industrial wall-bounded flows at high Reynolds number, the computational cost of LES is comparable to DNS when resolving the small vortical structures in the near wall region. To circumvent the prohibitive cost, the wall-modeled large eddy simulation (WMLES) is appealing. Following this approach, wall models are employed on a relatively coarse grid near wall to supply wall stresses as approximate boundary conditions to LES in outer flows.[1,3–6]

Numerous wall models have been developed since the pioneering works in the 1980s. Many of them simplify the low-pass filtered or ensemble-averaged momentum equation under the assumption of a quasi-parallel flow in the vicinity of the wall. The most commonly used wall model relies on the logarithmic law of the wall. It necessitates the near wall cells in which the wall model is used to be located in the inertial layer, which is usually unfeasible for industrial applications. Especially when using the immersed boundary method, the boundary conditions are imposed on staircase grid boundaries that are in general not aligned with the wall surfaces and distributed across a large range of the turbulent boundary layer (TBL), see Refs. 7–10. Empirical damping functions can be used to account for the viscous effects in the wall vicinity. Nonetheless the Newton's iterative method is required to determine the friction velocity u_τ. A suitable initial guess, usually taken from the previous solution, is crucial to ensure the convergence. The iterative process can be time-consuming for large-scale problems, even though the number of iterations is kept small. The acceleration of wall models has been a continuous research topic in wall-bounded turbulent flows and numerous models have been developed in the literature. The explicit power-law model[11] provides an alternative to the log-law, where a piecewise solution was also proposed to link to the viscous sublayer. Nevertheless, the buffer layer is not taken into account. Adaptive or hybrid algebraic wall models covering the entire inner layer of TBL are available, e.g., Refs. 12–16, but unfortunately none of them is explicit with respect to the friction velocity. More elaborated equation-based wall models have been proposed by solving the TBL equation on a separate refined grid, e.g., Refs. 17–19, which inevitably increase the computational overhead. Monfort *et al.*[20] introduced a meshless approach by numerical integration of the momentum equation along the wall normal direction. Yang *et al.*[21] presented an integral wall-model for LES for incompressible flows and Catchirayer *et al.*[22] later extended it to compressible and isothermal flows, where the von Kármán and Pohlhauseen integral method is used for integrating the boundary layer and consequently a small simple system needs to be solved iteratively for the free parameters. Nevertheless, the equation-based wall models are less efficient than the algebraic ones that can be also accurate as long as the outer layer is well resolved by LES.[5] Kalitzin *et al.*[23] suggested a tabulated approach in which the friction velocity is interpolated with a lookup table generated from a pre-computed fine solution. This approach is not very convenient and hence a versatile profile in closed form is sought. The current paper will present new implementations of the traditional algebraic wall models with the same accuracy but in an explicit way.

In this work, the key idea for developing explicit wall models is to express the non-dimensional quantities $u^+ = u/u_\tau$ or $y^+ = yu_\tau/\nu$

(with ν and y being the molecular viscosity and the wall distance, respectively) as a function of the local Reynolds number

$$Re_y = \frac{uy}{\nu} = u^+ y^+, \tag{1}$$

so that the friction velocity u_τ can be evaluated directly through

$$u_\tau = \frac{u}{u^+(Re_y)} \quad \text{or} \quad u_\tau = \frac{y^+(Re_y)\nu}{y}, \tag{2}$$

where the explicit formula for $u^+(Re_y)$ or $y^+(Re_y)$ will be derived shortly.

It is known that the inner region of the TBL can be decomposed into three parts: the viscous sublayer, the buffer layer, and the inertial layer. In the viscous sublayer, the following relation is found:

$$u^+ = y^+ = \sqrt{Re_y}. \tag{3}$$

In the inertial layer, the velocity profile obeys the logarithmic law

$$u^+ = \frac{1}{\kappa}\log(Ey^+) \quad \text{or} \quad y^+ = \frac{1}{E}e^{\kappa u^+}, \tag{4}$$

where $\kappa \approx 0.41$ and $E \approx 7.9$. Multiplying both sides of the second form of Eq. (4) by u^+ leads to the following relation between Re_y and u^+:

$$Re_y = \frac{u^+}{E}e^{\kappa u^+}. \tag{5}$$

Unfortunately, the inverse function is difficult to find. In the present work, the above formula is recast as

$$(\kappa E Re_y) = (\kappa u^+)e^{(\kappa u^+)}. \tag{6}$$

Denoting $x = \kappa E Re_y$ and $W = \kappa u^+$, one obtains

$$x = W(x)e^{W(x)}, \tag{7}$$

where $W(x)$ represents the Lambert W function that is implicitly defined as

$$W(x) = \log\left(\frac{x}{W(x)}\right). \tag{8}$$

Up to now, there is nothing new compared to the traditional log-law model but a change of variable. The key contribution of the present work is to expand the Lambert function $W(x)$ into series, e.g., the third-order expansion as follows:

$$W(x) \approx \log\left(\frac{x}{\log\left(\frac{x}{\log(x)}\right)}\right) = \log(x) - \log(\log(x) - \log(\log(x))). \tag{9}$$

This series converges for large x ($x > e$ with e being the natural number), namely,

$$Re_y = \frac{x}{\kappa E} > \frac{e}{\kappa E} \approx 0.8 \quad \text{or} \quad y^+ \gtrsim 0.9, \tag{10}$$

which obviously holds in the inertial layer. With the series expansion of the Lambert function, the following explicit version of the log-law is obtained:

$$u^+(Re_y) = \frac{1}{\kappa}W(\kappa E Re_y), \tag{11}$$

which still accurately matches the logarithmic behavior as illustrated in Fig. 1.

Alternatively for explicit wall models based on $y^+(Re_y)$, the classical log-law in the first form of Eq. (4) is multiplied to y^+ such that

$$Re_y = \frac{y^+}{\kappa}\log(Ey^+), \tag{12}$$

then

$$(\kappa E Re_y) = (Ey^+)\log(Ey^+). \tag{13}$$

Introducing $V = Ey^+$, the above formula becomes

$$x = V(x)\log V(x). \tag{14}$$

The Lambert function given in Eq. (7) can be easily recovered by setting $V(x) = e^{W(x)}$. Therefore, the alternative formula for the explicit log-law can be built on $y^+(Re_y)$ as follows:

$$y^+(Re_y) = \frac{1}{E}e^{W(\kappa E Re_y)}, \tag{15}$$

which shows a quasi-linear variation for large Re_y as observed in Fig. 2. Analogous to Spalding's law,[13] a unified expression for the entire inner layer can be given straightforward in the form of

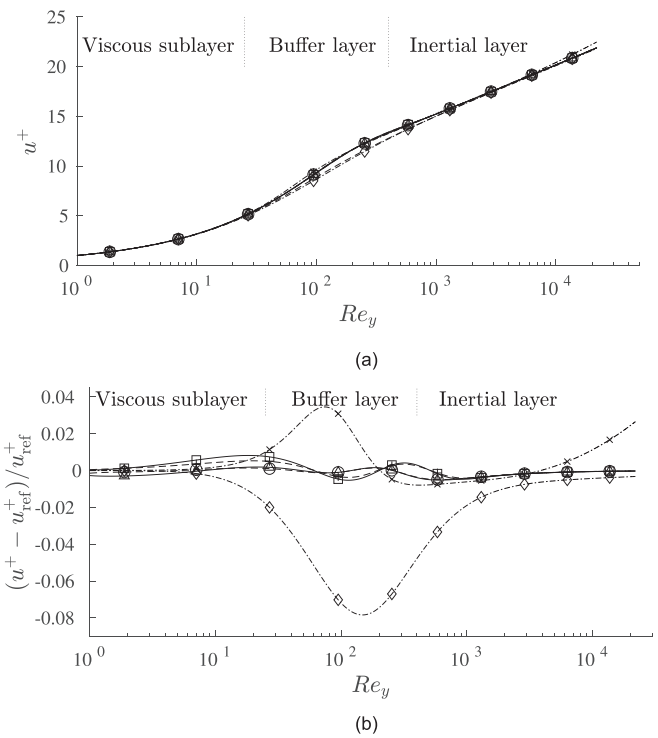

FIG. 1. Explicit wall functions based on $u^+(Re_y)$. (a) Comparison of profiles and (b) the relative error. - - -◇- - -, Model-I (16); —△—, Model-II (20); - - -◯- - -, Model-III (21); —□—, Model-IV (22); - - -+- - -, Model-V (23); ---×---, Model-VI (27); · · · · · ·, Spalart–Allmaras wall model (reference); - - - - Spalding wall model.

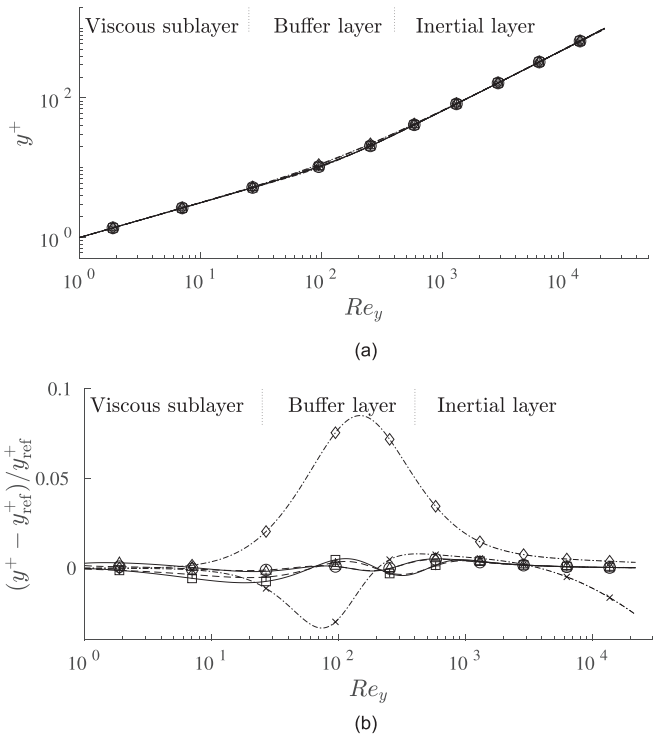

FIG. 2. Explicit wall functions based on $y^+(Re_y)$. (a) Comparison of profiles and (b) the relative error. - - -◇- - -, Model-I (16); —△—, Model-II (20); - - -◯- - -, Model-III (21); —□—, Model-IV (22); - - -+- - -, Model-V (23); --×--, Model-VI (27); · · · · · ·, Spalart–Allmaras wall model (reference); - - - - Spalding wall model.

- Model-I

$$y^+(Re_y) = \sqrt{Re_y + \frac{1}{E^2}\left(e^z - \sum_{n=0}^{9}\frac{z^n}{n!}\right)}, \quad z = 2W(\kappa E Re_y),$$
$$u^+(Re_y) = \frac{Re_y}{y^+(Re_y)}. \tag{16}$$

On the other hand, fully explicit wall models can be also achieved by blending the explicit profiles of the inertial layer and the viscous sublayer for the buffer layer with an appropriate fitting as follows:

$$u^+(Re_y) = (1-f)^p (Re_y)^{1/2} + f^p \frac{1}{\kappa}(\kappa E Re_y), \tag{17}$$

or

$$y^+(Re_y) = (1-f)^p (Re_y)^{1/2} + f^p \frac{1}{E} e^{(\kappa E Re_y)}, \tag{18}$$

where the damping function f approaches zero toward wall and unity far away, and such candidates could be

$$f = 1 - e^{-Re_y/s} \quad \text{or} \quad f = \tanh\frac{Re_y}{s}, \tag{19}$$

where s and p are the fitted parameters. The target profile could be extracted from DNS or wall-resolved LES results. In the present work, the analytical Spalart–Allmaras wall model[15] is selected for the purpose of using immersed boundary method for general applications, see Refs. 7–10. In this case, the new developed explicit wall models are used for computing u_τ at a reference point interior to fluid in the wall normal direction, and then at the boundary point, the Spalart–Allmaras wall model can be used directly for the tangential velocity. Therefore using the Spalart–Allmaras wall model for calibration can avoid inconsistency in the results. It should be noted that this is not the only choice, the constants can be easily adapted to different turbulence models for consistency matter as stressed in Ref. 23. The final expressions are listed as follows:

- Model-II

$$u^+(Re_y) = (e^{-Re_y/s})^p (Re_y)^{1/2} + (1 - e^{-Re_y/s})^p \frac{1}{\kappa} W(\kappa E Re_y),$$
$$y^+(Re_y) = \frac{Re_y}{u^+(Re_y)}, \quad p = 1.138, \quad s = 217.8. \tag{20}$$

- Model-III

$$y^+(Re_y) = (e^{-Re_y/s})^p (Re_y)^{1/2} + (1 - e^{-Re_y/s})^p \frac{1}{E} e^{W(\kappa E Re_y)},$$
$$u^+(Re_y) = \frac{Re_y}{y^+(Re_y)}, \quad p = 0.8632, \quad s = 232.1. \tag{21}$$

- Model-IV

$$u^+(Re_y) = \left(1 - \tanh\frac{Re_y}{s}\right)^p (Re_y)^{1/2} + \left(\tanh\frac{Re_y}{s}\right)^p \frac{1}{\kappa} W(\kappa E Re_y),$$
$$y^+(Re_y) = \frac{Re_y}{u^+(Re_y)}, \quad p = 1.214, \quad s = 97.77. \tag{22}$$

- Model-V

$$y^+(Re_y) = \left(1 - \tanh\frac{Re_y}{s}\right)^p (Re_y)^{1/2} + \left(\tanh\frac{Re_y}{s}\right)^p \frac{1}{E} e^{W(\kappa E Re_y)},$$
$$u^+(Re_y) = \frac{Re_y}{y^+(Re_y)}, \; p = 0.7894, \; s = 86.58, \tag{23}$$

where the constants given above are calibrated to the Spalart–Allmaras turbulence model, namely, they are computed by minimizing the error between the designed curve of $u^+ - Re_y$ (Model-II and Model-IV) or $y^+ - Re_y$ (Model-III and Model-V) to the target one (see Figs. 1 and 2).

Theoretically the expansion order of the Lambert function is crucial to the accuracy. In practice the sixth order expansion is found to be enough. It is important to note that above formulae are used for $\kappa E Re_y > e$ to ensure convergence of the expansion. Otherwise, Eq. (3) for the viscous sublayer should be used. Alternative solution without switching is to simply replace the Lambert W function by $W(\max(\kappa E Re_y, e))$ in the above formulae.

Werner and Wengle[11] initially proposed the power-law model for LES to approximate the logarithmic behavior in the inertial layer

$$u^+ = A(y^+)^{1/7}, \tag{24}$$

where $A \approx 8.3$. Even though the evaluation of power-law is explicit, it would be more interesting to obtain a fully explicit wall model containing the buffer layer. Motivated by Spalding's law,[13] the following new power-law is proposed:

$$y^+ = u^+ + D(u^+)^5 + C(u^+)^7, \tag{25}$$

where C and D are the constants to be calibrated, to match the velocity profile of the Spalart–Allmaras wall model[15] as well. The second term in the right hand side of (25) is used to enforce a similar asymptotic behavior of ν_t^+ to the Spalart–Allmaras wall model near wall. Multiplying both sides by u^+ yields

$$Re_y = (u^+)^2 + D(u^+)^6 + C(u^+)^8, \tag{26}$$

where the inverse formula can be found analytically for $u^+(Re_y)$ as follows:

- Model-VI

$$\begin{gathered}
u^+(Re_y) = \sqrt{-\frac{D}{4C} - \frac{1}{2}H + \frac{1}{2}\sqrt{\frac{D^2}{2C^2} - G + F + \frac{8C^2 + D^3}{4HC^3}}}, \\
y^+(Re_y) = \frac{Re_y}{u^+(Re_y)}, \\
H = \sqrt{\frac{D^2}{4C^2} + G - F}, \quad G = \frac{E}{3\sqrt{23}C}, \quad F = \frac{\sqrt{23}(D + 4CRe_y)}{CE}, \\
E = \left(27C - 27D^2Re_y + \sqrt{108(D + 4CRe_y)^3 + 729(C - D^2Re_y)^2}\right)^{1/3}, \\
C = 3.806 \times 10^{-7}, \quad D = -2.595 \times 10^{-5},
\end{gathered} \tag{27}$$

where $Re_y = \max(uy/\nu, 1.0 \times 10^{-12})$ is suggested.

The proposed wall models are compared in Figs. 1 and 2. It can be found that all the new formulas are close to target wall models. The Model-I (16) shows some deviations in the buffer layer as it is not fitted to the reference wall model. The Model-VI (27) gives a slightly better accuracy in the buffer zone, but the error increases with larger Re_y or y^+ where the power approximation becomes less suitable. The fitted wall models like Model-II (20), III (21), IV (22), and V (23) are almost identical to the Spalart–Allmaras wall model regardless of different damping functions. They are expected to produce the best accuracy, for which the maximum error is found far below 1%.

The LES of the turbulent plane channel flow is conducted for validating these wall models. The computational domain is taken to $2\pi\delta \times 2\delta \times 2\pi\delta$ similar to Refs. 24 and 25, with δ being the half channel width. The simulations are conducted under the Reynolds number $Re_\tau = u_\tau\delta/\nu = 2000$ and 5200 and compared to the DNS results of Lee and Moser.[26] Different grid resolutions are studied by varying the number of points per channel half width, $N = 10$, 20, and 30. The distance of the first grid point is taken to half of the grid size such that the grid resolution is $\Delta x^+ = \Delta y^+ = \Delta z^+ = 2y_1^+$, where a uniform grid is used throughout the work. For $Re_\tau = 2000$ the first grid point is located at $y_1^+ = Re_\tau/(2N) = 100, 50, 33.3$ for $N = 10$, 20, and 30, respectively. In the case of $Re_\tau = 5200$, one obtains $y_1^+ = 260$, 130, 86.7 for each grid.

The flow is computed using the hybrid recursive regularized density-based (HRR-ρ) lattice Boltzmann method (LBM)[27] along with the classical Smagorinsky subgrid model, where $C_s = 0.1$ and 0.14 are used for $Re_\tau = 2000$ and 5200, respectively. Periodic boundary conditions are assumed in the streamwise and spanwise directions while the wall shear stress is provided at walls by the proposed wall models. The flow is controlled dynamically by an external force in the streamwise direction such that the desired Reynolds number is achieved, $g = u_\tau^2/\delta + (u_\tau - u_\tau^{\text{avg}})/\Delta t$, where $u_\tau = \nu Re_\tau/\delta$ is the target value and u_τ^{avg} is the plane-averaged value from the computed solutions. Δt denotes the time step. It worth noting that the LBM works on the particle distribution functions instead of the macroscopic variables. Thus, special attention should be paid to their specifications at the boundaries. In the case of immersed boundary method, the second grid points serve as the reference points for u_τ and hence no interpolation error will affect the accuracy of the wall models. By assuming the constant friction velocity in the wall normal direction, the tangential velocity is determined at the boundaries, i.e., the first grid points. Quadratic profile is employed for the normal velocity as implied by the mass conservation at walls. The density is determined from the known particle distribution functions at the first grid points using the approach of Ref. 28. The RANS mixing length model is used for the eddy viscosity at the first grid points with the van Driest near wall

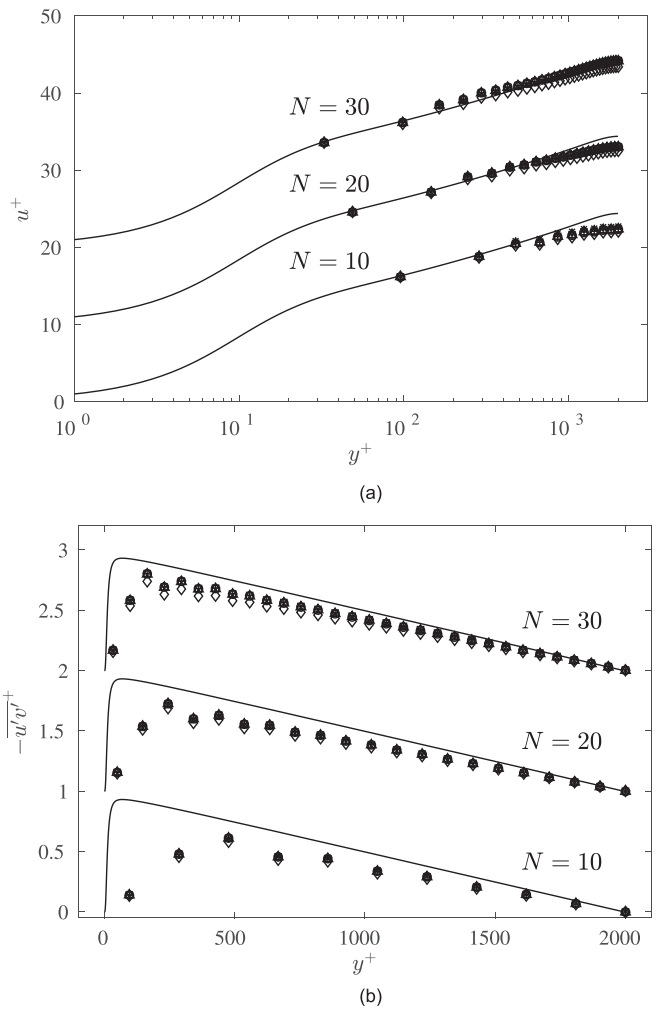

FIG. 3. Profiles of the normalized mean velocity u^+ (a) and the normalized resolved Reynolds stress $-\overline{u'v'}^+$ (b) at $Re_\tau = 2000$. - - -◇- - -, Model-I (16); —△—, Model-II (20); - - -◯- - -, Model-III (21); —□—, Model-IV (22); - - -+- - -, Model-V (23); --×--, Model-VI (27); ——, DNS results of Lee and Moser.[26] The figures are shifted vertically for better visualization.

damping as in Ref. 24. Finally, all the particle distribution functions are reconstructed from those macroscopic quantities using the equilibrium approach[25] and the collision occurs to advance in time.

Figures 3 and 4 show the profiles of the normalized mean velocity u^+ and the normalized resolved Reynolds stress $-\overline{u'v'}^+$ at $Re_\tau = 2000$ and 5000, respectively. It is seen that the results are close to each other for all the proposed wall models and agree well with the DNS data of Ref. 26. It confirms the validity of the proposed explicit wall models and the use of LBM for wall-modeled LES at high Reynolds number. A small difference is found for the Model-I (16) at $Re_\tau = 2000$ on the fine grid $N = 30$ where the first grid points lie in the buffer region, which is due to the fact that the Model-I (16) is not fitted to any existing models. The difference becomes negligible on coarser grids or at higher Reynolds number $Re_\tau = 5200$. Some discrepancies are also found for the Model-VI (27) at $Re_\tau = 5200$ on the coarse grid $N = 10$ where the first grid points reach around $y_1^+ = 260$ or $Re_y \approx 5000$, above which the power

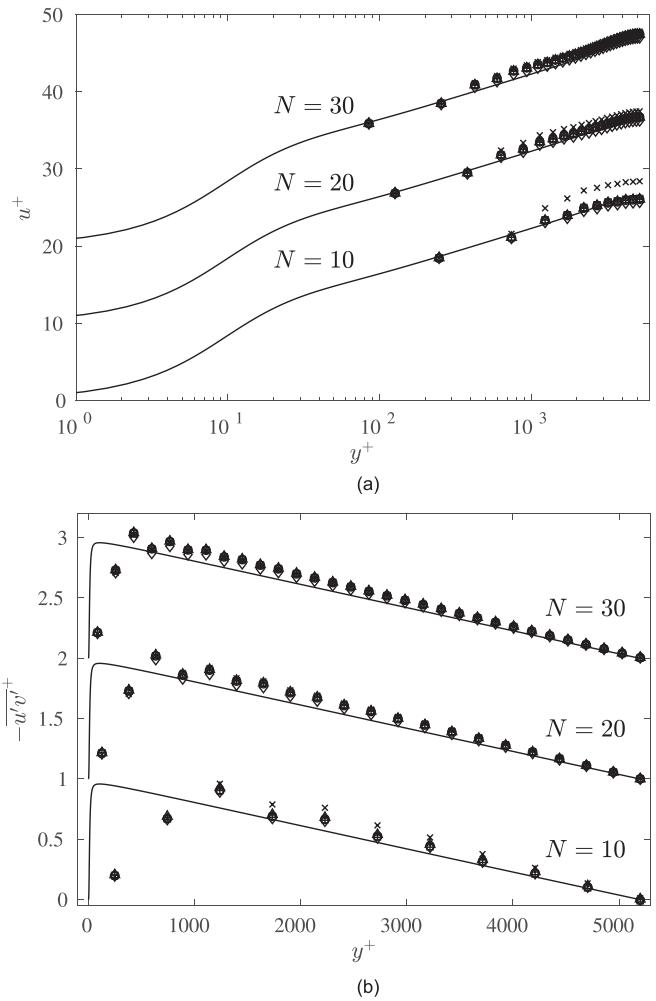

FIG. 4. Profiles of the normalized mean velocity u^+ (a) and the normalized resolved Reynolds stress $-\overline{u'v'}^+$ (b) at $Re_\tau = 5200$. - - -◇- - -, Model-I (16); —△—, Model-II (20); - - -◯- - -, Model-III (21); —□—, Model-IV (22); - - -+- - -, Model-V (23); --×--, Model-VI (27); ——, DNS results of Lee and Moser.[26] The figures are shifted vertically for better visualization.

approximation of the logarithmic behavior is actually less accurate as demonstrated in Figs. 1 and 2. Nevertheless, the fitted log-law wall models, as Model-II (20), III (21), IV (22), and V (23), give almost indistinguishable results with respect to various forms of the damping functions. In terms of computational cost, even though the proposed explicit wall models are found slightly more expensive than a single Newton iteration in classical implicit wall models, their overall performance is obvious since the iterative models generally require several iterations to converge. It appears that the Model-VI (27) involving many square-root operations is computationally intensive, and it is in fact as efficient as the others as it does not include any damping functions that may be computationally expensive. Finally, for the accuracy and efficiency point of view, the fitted log-law is highly recommended and general applications will be considered in the future work.

This work was supported by DGAC Project No. 2018–16 OMEGA3 and ANR Industrial Chair ALBUMS (Grant No. ANR-18-CHIN-0003–01). Centre de Calcul Intensif d'Aix-Marseille is acknowledged for granting access to its high performance computing resources. This work was performed using HPC resources from GENCI-TGCC (Grant 2021-A0092A07679). We wish to acknowledge helpful discussions with Jérôme Jacob.

DATA AVAILABILITY

Data sharing is not applicable to this article as no new data were created or analyzed in this study.

REFERENCES

[1]P. Sagaut, *Large Eddy Simulation for Incompressible Flows. An Introduction*, Scientific Computation, 3rd ed. (Springer, 2006).
[2]P. Sagaut, S. Deck, and M. Terracol, *Multiscale and Multiresolution Approaches in Turbulence*, 2nd ed. (Imperial College Press, 2013).
[3]U. Piomelli and E. Balaras, "Wall-layer models for large-eddy simulations," Annu. Rev. Fluid Mech. **34**, 349–374 (2002).
[4]U. Piomelli, "Wall-layer models for large-eddy simulations," Prog. Aerosp. Sci. **44**, 437–446 (2008).
[5]J. Larsson, S. Kawai, J. Bodart, and I. Bermejo-Moreno, "Large eddy simulation with modeled wall-stress: Recent progress and future directions," Mech. Eng. Rev. **3**, 15–00418 (2016).
[6]S. T. Bose and G. I. Park, "Wall-modeled large-eddy simulation for complex turbulent flows," Annu. Rev. Fluid Mech. **50**, 535–561 (2018).
[7]F. Roman, V. Armenio, and J. Frohlich, "A simple wall-layer model for large eddy simulation with immersed boundary method," Phys. Fluids **21**, 101701 (2009).
[8]S. Wilhelm, J. Jacob, and P. Sagaut, "An explicit power-law-based wall model for lattice Boltzmann method-Reynolds-averaged numerical simulations of the flow around airfoils," Phys. Fluids **30**, 065111 (2018).
[9]S. Wilhelm, J. Jacob, and P. Sagaut, "A new explicit algebraic wall model for les of turbulent flows under adverse pressure gradient," Flow, Turbul. Combust. **106**, 1–35 (2021).
[10]S.-G. Cai, J. Degrigny, J.-F. Boussuge, and P. Sagaut, "Coupling of turbulence wall models and immersed boundaries on Cartesian grids," J. Comput. Phys. **429**, 109995 (2021).
[11]H. Werner and H. Wengle, "Large-eddy simulation of turbulent flow over and around a cube in a plate channel," in *Turbulent Shear Flows 8* (Springer, Berlin, Heidelberg, 1993), pp. 155–168.
[12]H. Reichardt, "Vollständige Darstellung der turbulenten Geschwindigkeitsverteilung in glatten Leitungen," Z. Angew. Math. Mech. **31**, 208–219 (1951).
[13]D. B. Spalding, "A single formula for the law of the wall," J. Appl. Mech. **28**, 455–458 (1961).
[14]A. J. Musker, "Explicit expression for the smooth wall velocity distribution in a turbulent boundary layer," AIAA J. **17**, 655–657 (1979).

[15]S. R. Allmaras, F. T. Johnson, and P. R. Spalart, "Modifications and clarifications for the implementation of the spalart-allmaras turbulence model," in Proceedings of 7th International Conference on Computational Fluid Dynamics, ICCFD7-1902 (2012).
[16]T. Knopp, T. Alrutz, and D. Schwamborn, "A grid and flow adaptive wall-function method for RANS turbulence modelling," J. Comput. Phys. **220**, 19–40 (2006).
[17]E. Balaras, C. Benocci, and U. Piomelli, "Two-layer approximate boundary conditions for large-eddy simulations," AIAA J. **34**, 1111–1119 (1996).
[18]J. Bodart and J. Larsson, "Wall-modeled large eddy simulation in complex geometries with application to high-lift devices," in *Annual Research Briefs* (Center for Turbulence Research, 2011).
[19]S. Kawai and J. Larsson, "Wall-modeling in large eddy simulation: Length scales, grid resolution, and accuracy," Phys. Fluids **24**, 015105 (2012).
[20]D. Monfort, S. Benhamadouche, and P. Sagaut, "Meshless approach for wall treatment in large-eddy simulation," Comput. Methods Appl. Mech. Eng. **199**, 881–889 (2010).
[21]X. I. A. Yang, J. Sadique, R. Mittal, and C. Meneveau, "Integral wall model for large eddy simulations of wall-bounded turbulent flows," Phys. Fluids **27**, 025112 (2015).
[22]M. Catchirayer, J.-F. Boussuge, P. Sagaut, M. Montagnac, D. Papadogiannis, and X. Garnaud, "Extended integral wall-model for large-eddy simulations of compressible wall-bounded turbulent flows," Phys. Fluids **30**, 065106 (2018).
[23]G. Kalitzin, G. Medic, G. Iaccarino, and P. Durbin, "Near-wall behavior of RANS turbulence models and implications for wall functions," J. Comput. Phys. **204**, 265–291 (2005).
[24]O. Malaspinas and P. Sagaut, "Wall model for large-eddy simulation based on the lattice Boltzmann method," J. Comput. Phys. **275**, 25–40 (2014).
[25]M. Haussmann, A. C. Barreto, G. L. Kouyi, N. Rivière, H. Nirschl, and M. J. Krause, "Large-eddy simulation coupled with wall models for turbulent channel flows at high reynolds numbers with a lattice boltzmann method - Application to coriolis mass flowmeter," Comput. Math. Appl. **78**, 3285–3302 (2019).
[26]M. Lee and R. D. Moser, "Direct numerical simulation of turbulent channel flow up to $Re_\tau \approx 5200$," J. Fluid Mech. **774**, 395–415 (2015).
[27]J. Jacob, O. Malaspinas, and P. Sagaut, "A new hybrid recursive regularised Bhatnagar-Gross-Krook collision model for Lattice Boltzmann method-based large eddy simulation," J. Turbul. **19**, 1–26 (2018).
[28]Q. Zou and X. He, "On pressure and velocity boundary conditions for the lattice boltzmann bgk model," Phys. Fluids **9**, 1591 (1997).